Accepted Manuscript

Seismogenesis and earthquake triggering during the 2010–2011 Rigan (Iran) earthquake sequence

Hiwa Mohammadi, Thomas J. Bayliss, Esmaeil Nekouei Ghachkanlu

PII: S1464-343X(16)30378-8

DOI: 10.1016/j.jafrearsci.2016.11.019

Reference: AES 2732

To appear in: *Journal of African Earth Sciences*

Received Date: 10 March 2016

Revised Date: 7 November 2016

Accepted Date: 18 November 2016

Please cite this article as: Mohammadi, H., Bayliss, T.J., Nekouei Ghachkanlu, E., Seismogenesis and earthquake triggering during the 2010–2011 Rigan (Iran) earthquake sequence, *Journal of African Earth Sciences* (2016), doi: 10.1016/j.jafrearsci.2016.11.019.

Seismogenesis and earthquake triggering during the 2010–2011 Rigan (Iran) earthquake sequence

Corresponding Author: **Hiwa Mohammadi**

Order of Authors: Hiwa Mohammadi [1], Thomas J. Bayliss [2], Esmaeil Nekouei Ghachkanlu[1]

1. **Department of Earth Sciences, College of Sciences, Shiraz University, Shiraz, Iran**

E-mail: Hiwa.2006.waran@gmail.com

2. **Seismic Risk Group, School of Environmental Sciences, University of East Anglia, Norwich, Norfolk NR4 7TJ, United Kingdom.**

Abstract

This study assesses the aftershock activity of two earthquakes that occurred on December 20, 2010 with magnitude of M_N 6.5 (Global CMT M_w 6.5) and January 27, 2011 with magnitude of M_N 6.0 (Global CMT M_w 6.2) in the Rigan region of southeastern Iran. This study has been done by assessing the statistical properties of the aftershock sequences associated with each of these earthquakes, namely *b*-value of Gutenberg–Richter relation, partitioning of radiated seismic energy, *p*-value of modified Omori law and the D_C-value associated with the fractal dimension. The *b*-values of *b*=0.89±0.08 and *b*=0.88±0.08 were calculated for first main shock and second main shock sequence respectively. This suggests that this region is characterized by large differential stress; the genesis of large aftershock activity in a short time interval gives power this. Further, 2.2% of the whole energy is related with the aftershocks activity for first main shock sequence while 97.8% is associated with main shock; for second sequence , 20% of the total energy is associated with the aftershocks activity while 80% is associated with main shock. The *p*-values of 1.1±0.12 and 1.1±0.1 were calculated for first and second main shocks sequence respectively, which imply fast decay rate of aftershocks and high surface heat flux. A value of the spatial fractal dimension (D_c) equal to 2.34 ± 0.03 and 2.54 ± 0.02 for first and second main shocks sequence respectively, which reveals random spatial distribution and source in a two-dimensional plane that is being filled-up by fractures. Moreover, we then use the models to calculate the Coulomb stress change to appraise coming seismic hazard by inspecting the static Coulomb stress field due to these two main shocks for the recognition of the conceivable regions of aftershocks activity. The first main shock increased stress by more than 0.866 bars at the hypocenter of the second main shock, thus promoting the failure. In addition, the cumulative

coseismic Coulomb stress changes due to the reveals that most of the aftershocks happened in the region of increased Coulomb stress.

Keywords: Rigan, Statistical properties of aftershocks, *b*-value, partitioning of radiated seismic energy, Omori law, spatial fractal dimension (D_c), Coulomb failure stress.

1. Introduction

On December 20, 2010 at 22:12 local time, a moderately-sized earthquake of M_N 6.5 (Global CMT M_w 6.5) took place near Rigan in southeastern Iran. Thirty-eight days later, another moderately-sized earthquake M_N 6.0 (Global CMT M_w 6.2) occurred nearby on January 27, 2011 at 12:09 local time on January 27 2011. The Rigan area is located in southeastern Iran, at the southern segment of the Lut block and the northern border of the Jazmourian depression (Fig. 1). The first main shock resulted in four deaths, all in the low settlement of Chah Qanbar; no casualties were narrated from the 2011 event (Walker et al. 2013). The historical seismicity (Fig. 1) of this area is limited to the earthquakes reported after 1800 A.D. (Ambraseys and Melville, 1982; Berberian, 1995). Berberian (1995) suggests evidence may be present for historical earthquakes around Koohbanan, Zarand, Kerman, Bam and Mahan caused by active faults near them. Important historical earthquakes are the Nosrat-Abad (1838), Hoorjand (November, 1854), Chatrood (January, 17, 1864), Chatrood (August, 4, 1871) and Sirch (1877). The M_S = 7.0 Nosrat-Abad earthquake was a shock followed by two years of aftershocks. The M_S= 5.8 (MMI = VII+) Hoorjand earthquake destroyed some villages located northeast of Kerman. More recently Iranian seismic activity has been documented on in-situ recording equipment, notably

during the 2003 Bam (M_w=6.6) and 1998 (M_S=5.3) earthquakes with known mechanisms and the 1923 (M_S=5.6) with unknown focal mechanism which related to the Kahourak fault.

The Lut block is placed in southeastern Iran and expands approximately 200 km east to west and almost 900 km north to south, and is commonly regarded as a non-deforming tectonic structure. It is bordered to the south by the Jazmourian depression, to the north by the Doruneh fault, to the west by the Nayband fault and the Gowk fault system and the Nehbandan fault system in the east (Hessami and Jamali, 2006). The Gowk, Sabzevaran, Bam, Jiroft and the Nehbandan (including Kahurak F., southwest termination) fault zones are the seismically active fault systems close to the epicentral area considered in this study. Rezapour and Mohsenpur (2013) state that December 20, 2010 Rigan earthquake started by enactment of a dextral fault in the upper crust. They also state that the geometries of the conceivable activated fault planes match the Kahurak and Bam faults in the area, while a clear alignment of the epicentral distribution of the aftershocks recorded by the temporary seismic network are consistent with the Kahurak fault trend. However, Ashtari-Jafari (2011) determined that the first main shock happened on a hidden earthquake fault, running approximately parallel to the Bam earthquake fault, and he recommended the name 'Rigan earthquake fault' for this new fault. These events provide opportunity to further understand the distribution of active faults in the region and the seismic hazard local populations may be subject to. The earthquakes additionally offer a new perception into the active tectonics of this region as well as 2003 Bam earthquake (M_w =6.6).

Many estimates of the locations of each main shock have been made. The Institute of Geophysics at University of Tehran (IGUT) estimated the locations using their permanent seismic stations-at 28.44^{o}N and 59.15^{o}E for the first main shock, and second main shock at 28.294^{o}N and 58.95^{o}E. The focal mechanism solutions from different seismological agencies

were published after the both main shocks occurred. Walker et al. (2013) used interferometry and teleseismic body waveform and surface displacements from Synthetic Aperture Radar (SAR) interferometry to suggest the 2010 main shock induced with a right-lateral strike-slip motion on a formerly near-vertical fault with a strike of ~210°N;, and that the 2011 main shock induced with a left-lateral strike-slip motion on another near-vertical fault with strike of ~310°N. While they successfully identified a series of tiny cracks and en-echelon fissures that appeared after these earthquakes, neither event created a good visible surface trace in the region. However, U.S. Geological Survey's (USGS) solution was to suggest a right lateral strike-slip including a reverse component; the Global Centroid Moment Tensor (Global CMT) solution for the first main shock provided by the Harvard group is in agreement with a pure dextral strike-slip motion. Based on USGS and Global CMT outcomes, northeast–southwest and trends northwest–southeast were proposed for nodal planes.

Earthquakes are typically followed by increased seismic activity, identified as 'aftershocks', which last for several days to several years. They are also subject to complicated triggering mechanisms which move in a highly heterogeneous system of non-linearly cooperation faults incorporated in a visco-elastic medium (Ben-zion, 2008); relaxation of these stresses motivates aftershocks (Rybicki, 1973; Mendoza and Hartzell, 1988; King et al., 1994; Hardebeck et al., 1998). This analysis evaluates aftershock activity using a range of statistical properties of aftershock sequences (*b*-value of Gutenberg–Richter relation, partitioning of radiated seismic energy, *p*-value of modified Omori law, and D_C- value of fractal dimension) in order to shed light on the seismotectonic properties of the study area. In addition, an attempt has been made to assess future seismic hazard by examining the static Coulomb stress field due to

coseismic slip of both main shocks for the identification of the possible regions of aftershocks activity.

2. Tectonic Setting

The Alpine–Himalayan belt in Iran is represented by a wide band of diffused seismicity and includes a few mobile belts encompassing little and fairly steady blocks. Berberian (1976) separated Iran into four major seismotectonics zones, one of which is the major component of the Central Iranian Block, which includes of the Lut , Poshte Badam, Yazd and Tabas blocks. The boundaries among these blocks are strike slip faults, the blocks have been liable to extensive counter-clockwise rotation. Also, the fault systems in this region are varied from those in other parts of Iran because of the orientation and geometric specification of the faults; for example, they are linear, long, and narrow (Hessami and Jamali, 2006). The latest dynamic deformation in the east central Iran is overwhelmed by major N–S or NNW–SSE right-lateral strike slip faulting with some NW–SE reverse faults and some E–W left-lateral strike–slip faults. The northward movement of central Iran in respect to western Afghanistan results in local scale right-lateral shear across the eastern border of Iran, which is located south of latitude 34◦N on N–S right-lateral faults that surround the Dasht-e-Lut (Walker and Jackson, 2004; Meyer and Le Dortz, 2007). The Central Iran is not considered a linear seismic zone. It is portrayed by scattered seismic movement with large-Earthquakes generated in central Iran are typically shallow focus (less than 25 km) and are normally associated with surface faulting (Berberian, 1976). The 2010 and 2011 Rigan earthquakes occurred in the low-lying and sparsely inhabited Narmashir desert district region south of the Dasht-e-Lut desert. This region is flanked toward the south by the

Shahsavaran mountains mountain chain. The epicentral region of these events was situated between the southern Lut Block and the Makran–Jazmourian Depression. Various large earthquakes happened on the right-lateral strike–slip fault systems along the western edge of Dasht-e-Lut. Walker (2006) proposed that Late-Quaternary thrust faulting and strike-slip faulting occurred inside of the area, that regional faults are imperative to allow exchange of tectonic strain by appropriating a part of the right-lateral shear among the Makran-Zagros districts along the right lateral fault systems toward the central parts of Iran.

3. Rigan main shocks and their aftershock sequence

The earthquake catalogue used in the current study is taken from the Iranian Seismological Center of the Institute of Geophysics at University of Tehran (IGUT; http://irsc.ut.ac.ir/bulletin.php/). An earthquake data set used in seismicity or seismic hazard studies surely should be homogenous. In other words, it is indispensable to apply the equal magnitude scale in seismic analyzes. The IGUT reported earthquakes on the corrected Nuttli (1973) magnitude (M_N) scale. However, the study area is located in the SE of Iran between longitudes of 57.00-59.00°E and latitudes of 28.00-29.00°N on which the events occurred. Figure 2 shows the epicenter locations of the main shocks and their aftershocks. This sequence consists of 256 earthquakes of $2.6 \leq M_N \leq 6.5$ recorded by IGUT during the period December 20, 2010 to April 6, 2011. Figure 3a displays the cumulative number of earthquakes with $M_N \geq 2.6$ in the catalog. The seismicity rate has a sharp change after the first main shock (red star in Fig. 2) which occurred on December 20, 2010 with M_N=6.5 and at the second main shock which occurred on January 27, 2011 with magnitude M_N= 6.0 (Yellow Star in Fig.2) due to the Rigan

aftershock sequence. Figure 3b illustrates magnitude of events versus time. We can see that there are two main clusters in this sequence, each occurring in the days following each of the main shocks considered in this work. Thus, here we defined two sequences, first sequence has been considered after occurrence December 20, 2010 till before occurrence second main shock and second sequence has been considered after occurrence second main shock from January 27, 2011 till 6 April 2011. Most of the aftershocks from first main shock are clustered in the NE to SW direction (Fig. 3c) coinciding with the strike of one of the nodal plane (np1 strike = 36, dip = 87, rake = 180) of the first main shock's fault plane solution reported in the Global CMT catalogue. IGUT reported 15 aftershocks of magnitude $M_N \geq$ 4.0 within first sequence which mainly declusterd NE to SW (Fig. 3c). The occurrence of such larger magnitude aftershocks in any aftershock sequence suggests that large asperities exist in the rupture zone of main shock from where seismic energy is released in the form of moderate size aftershocks. Also, aftershocks associated with the second main shock are mainly declustered in the NW to SE direction (Fig. 3d) coinciding with the strike of one of the nodal plane (np1 strike = 129, dip = 77, rake = −5) of the second main shock's fault plane solution reported in the Global CMT catalogue. IGUT reported 17 aftershocks of magnitude $M_N \geq$4.0 within this sequence and mainly declusterd NW to SE. Also, Walker et al. (2013) state that the causative fault of the December 20, 2010 has NE to SW direction and January 27, 2011 Rigan earthquakes has NW to SE direction.

4. Statistical properties of the aftershock sequence

4.1. Frequency–magnitude scaling relationship

181 The quantity *N* of earthquakes with magnitudes larger than or identical to *M* is approximated by
182 using the relation (Gutenberg and Richter, 1944):
183
184 $$log_{10}N_m = a_m - bM \qquad (1)$$
185
186 where N_m is the cumulative number of earthquakes with magnitudes equal to or large than *M*, *b*
187 depicts the slope of the size distribution of events, and *a* is corresponding to the seismicity rate.
188 Appraisals of *b*-value intimate a fractal relation among frequency of occurrence and the radiated
189 energy, seismic moment or fault length, and this is one of the most extensively used statistical
190 parameters to explain the scale scaling properties of seismicity. The *b*-value for the most part
191 fluctuates from 0.5 to 1.5 contingent upon the tectonic setting, tectonic stress and the magnitude
192 ranges, but regularly approaches to 1 for seismically active regions. The variety of *b*-value can
193 be identified with the stress distribution after the main shock, as well as the history of previous
194 ruptures. Spatial and temporal varieties in *b*-values are distinguished to reflect the stress field, for
195 the *b*-value is conversely reliant on differential stress (Scholz 1968; Ogata et al., 1991; Urbancic
196 et al., 1992; Ogata and Katsura, 1993; Narteau et al., 2009). Schrolemmer et al. (2005) state that
197 the *b*-value is additionally subject to styles of faulting, as the *b*-values of thrust faults are the
198 lowest among the three types of faulting mechanisms, which can be considered as confirmation
199 of the relationship between *b*-value and stress. Areas with lower *b*–value are likely to be areas
200 under higher applied shear stress after the main shock, while the areas with higher *b*–value are
201 areas that encounter slip. Estimation of reliable *b*-values is reliant on a clearly defined time
202 interval of catalogued seismicity.

There are many techniques to estimation *b*-value; yet the most powerful and generally acknowledged technique for estimation of *b*-value is the Maximum Likelihood Method (MLM). The *b*-value of a region can be assessed from the aftershock sequence data utilizing the hypothetical thought given as Utsu (1965):

$$b = \frac{Log_{10}e}{M_{mean} - M_c} \qquad (2)$$

As shown in Fig. 4, the cut-off magnitude (M_c) for the both sequences was calculated to be equal to 3.2 with 90% goodness of fit level (Fig. 4); the frequency-magnitude statistics of theses aftershocks sequence were modeled using the GR scaling relation. For the first aftershock sequence, from December 20, 2010 to January 27, 2011, b=0.89 $\pm$ 0.08 and a=4.77 (Fig. 4a) were calculated; similarly, b=0.88 $\pm$ 0.08 and a=4.86 (Fig. 4b) were calculated for the second main shock sequence. The *b*-value in both sequences are lower than the global mean value of 1.0, suggesting that the two sequences are subject to larger magnitude aftershocks and high differential crustal stress in the regime.

4.2. Energy partitioning

Utsu (2002) claims that the level of aftershocks is chiefly related with the size of main shock in a seismic sequence. The stress situation and heterogeneity of rock mass influences the change in size (Δm) between magnitude of main shock (M_{ms}) and its biggest aftershock. In its unique structure, Båth's law expresses that the difference Δm between a given main shock with magnitude M_{ms} and its biggest aftershock magnitude is constant, independent of the main shock magnitude (Båth, 1965). However, in spite of extensive research about the statistical variability

of Δm (Vere-Jones, 1969; Kisslinger and Jones, 1991; Console et al., 2003), the validity of the law remains an open issue (Vere-Jones, 1969; Vere-Jones et al., 2005). This study aims to derive the biggest aftershock magnitude from the Gutenberg-Richter law and fit it into the standard view of Bath's law following Shcherbakov and Turcotte (2004).

The magnitude of the biggest aftershock consistent with Gutenberg-Richter relationship for aftershocks is obtained by assuming $N\ (\geq m) = 1$ which yields $a = bm^*$. If Båth's law is applicable to the inferred magnitude m^* the Gutenberg–Richter relationship takes the following form:

$$log_{10}N(\geq M) = b(M_{ms} - \Delta m^* - M) \quad (3)$$

where $\Delta m = M_{ms} - M^*$. The energy E radiated throughout an earthquake is associated empirically to its moment magnitude M by (Utsu, 2002)

$$log_{10}E(M) = \frac{3}{2}M + log_{10}E_0 \quad (4)$$

With, E_0 = 6.3 × 104 Joules.

This relation is applied directly to describe the link among the energy radiated by the main shock E_{ms} and the moment magnitude of the main shock M_{ms},

$$E_{ms} = E_0.10^{\frac{3}{2}m_{ms}}$$

Shcherbakov and Turcotte (2004) state that the proportion of the whole radiated energy by the aftershocks E_{as} to the whole energy radiated by the main shock E_{ms} is given by

$$\frac{E_{as}}{E_{ms}} = \frac{b}{\frac{3}{2}-b} 10^{-\frac{3}{2}\Delta m} \quad (5)$$

Assuming that all earthquakes have the same seismic efficiency, the share of the radiated energy to the whole is saved as elastic energy is also the proportion of the drop within the stored elastic power due to the aftershocks to the drop in the stored elastic energy because of the main shock. Shcherbakov in et al. (2005) determined the fraction of entire energy associated with aftershocks can be written as

$$\frac{E_{as}}{E_{ms}+E_{as}} = \frac{\frac{b}{\frac{3}{2}-b} 10^{-\frac{3}{2}\Delta m}}{1+\frac{b}{\frac{3}{2}-b} 10^{-\frac{3}{2}\Delta m}} \quad (6)$$

Therefore, by considering a = 4.77 and b = 0.89 for first sequence and a = 4.86 and b = 0.88 for second sequence which computed from G–R relationship, the modified magnitude for the largest aftershock (M^*) as 5.3 and 5.5 for the first and second sequences respectively. Moreover, magnitude difference (Δm^*) as 1.2 and 0.5 for first and second sequences respectively. We found that 2.2% of the whole energy is related with the for first sequence's aftershock activity while 97.8% is associated directly with main shock. In comparison, 20% of the total energy is associated with the aftershock activity from the second sequence while 80% is associated with main shock.

4.3. Temporal decay of aftershock events

Aftershock activity will decay over time in a quasi-hyperbolic manner. This decay is typically described by using a relation known as the changed Omori law (Utsu et al., 1995; Ben-Zion, 2008) expressed inside the equation:

$$n(t) = k(t+c)^{-p} \qquad (7)$$

where n(*t*) is the occurrence rate of aftershocks (number of shocks/day), *t*-days after the main shock; *k*, *c* and *p* are positive constants. To determine those parameters, it is common to make use of the cumulative range of aftershocks (Utsu, 2002) inside the form:

$$N(t) = \frac{k\left[c^{1-p} - (t+c)^{1-p}\right]}{p-1} \quad for\ p \neq 1 \qquad (8)$$

where *N(t)* is the cumulative number of aftershocks *t*-days after the main shock. However, the most important is generally considered to be *p*, with $p = 1$ in the original version of the Omori law. According to Olssen (1999) and Utsu et al. (1995), *p* changes between 0.5 and 1.8, and this parameter varies from sequence to sequence based to tectonic situation in the examined area. In this manner, more consideration is paid in the estimation *p* utilizing the maximum likelihood as suggested by Nyffengger and Frolich (1998, 2000). *k* is controlled by aggregating the number of events in the sequence. *c* which usually approximates to zero, is a dubious parameter (Utsu et al., 1995) and is dependent on the rate of activity in the beginning part of the sequence. Clearly, if c = 0, *n(t)* in Eq. (7) diverges at $t = 0$. According to Yamakawa (1968), higher values for c ($c \geq 0.01$ days) imply more complex capabilities of the rupture process of the main shock. Whilst p is sort of unbiased of the threshold magnitude, M_c, *c* often suggests tight dependence on M_c (Utsu, 2002). This is probably because of missing data shortly after the main shock when considerable small aftershocks are not seen on reported records. The reason for fluctuating values of *p* in the crust is inadequately known. Moreover, the aftershock decay is thought to mirror the strain readjustment following the strain changes because of the main shock (Ben-Zion, 2008). Stress readjustment can be considered to mirror the complicated relaxation processes (Stein and

292 Wysession, 2002), and structural heterogeneity within the source volume (Kisslinger and Jones,
293 1991; Utsu et al., 1995) associated to the tectonic structure of the region.

294 The maximum likelihood method was applied to estimate the value of *p* of Eq. (7) for the
295 aftershock sequence of the Rigan sequence shown in Fig. 5. The *p*-values of 1.1 ± 0.12 (Fig.
296 5a) and 1.1 ± 0.1 (Fig. 5b) were calculated for the first and second sequence respectively. The
297 *p*-values are higher value compared to the usual values of the order of 1.0 (Fig. 5). Bowman
298 (1997) determined that the temporal decay of aftershock activity indicates the strain scattering
299 with time in the aftershock region for intraplate earthquakes in Australia. Kisslinger and Jones
300 (1991) related high *p*-values to high estimations of heat flow for California and proposed that
301 higher temperature created abbreviated stress slackening times for the fault zone.

302

303 **4.4. Spatial fractal dimension**

304

305 Seismicity is a classical instance of a complicated phenomenon that may be quantified the usage
306 of fractal theory (Turcotte, 1997). Specifically, epicenter distributions and fault networks have
307 fractal properties (Goltz, 1998). The fractal dimension (D) qualities are evaluated utilizing the
308 connection dimension. The correlation dimension as characterized by Grassberger and Procaccia
309 (1983) measures the spacing of the set of points, which in this example are the earthquake
310 epicenters and is given as:

311

312 $$D_c = \lim_{r \to 0} [logC(r)/logr] \qquad (9)$$

313

where C(r) is the correlation function. The correlation function measures the clustering or spacing of a set of factors, here the earthquake epicenters, and is given via the relation:

$$C(r) = \frac{2}{N(N-1)} N(R < r) \qquad (10)$$

where N(R/r) is the number of pairs (Xi, Xj) with a smaller distance than *r*. Should the epicenter dispersion have a fractal structure, the subsequent relation is acquired

$$C(r) \sim r^{D} \qquad (11)$$

where *D* is a fractal dimension, more strictly, the correlation dimension (Grassberger and Procacci, 1983). The usage of this relation the fractal dimension of spatial distribution of the earthquakes is evaluated. By plotting C(r) towards r on a double logarithmic coordinate, the fractal size *D* is detrermined by the graph's slope. The distance r between two events, $(\Theta 1, \phi 1)$ and $(\Theta 2, \phi 2)$, is calculated by using a spherical triangle as given by Hirata (1989):

$$r = cos^{-1}\left[cos\Theta 1 cos\Theta 2 + sin\Theta 1 sin\Theta 2 cos(\phi 1 - \phi 2)\right] \qquad (12)$$

The slope is obtained by fitting a least-square line in the scaling region.

The spatial fractal dimension for the Rigan sequence is calculated from the double-logarithmic plot of the correlation integral and distance between hypocenters (Fig. 6), and found to be equal to 2.34 ± 0.03 (Fig. 6a) and 2.54 ± 0.02 (Fig. 6b) for the first and second sequence respectively. The D_c-value is larger than 2.0 in both sequences, indicating that the

events are randomly distributed into the fault zone crustal volume, whereas much of this volume seems free from hypocenters.

5. Static Coulomb-stress changes

In recent years, various studies have investigated the Coulomb stress change to clarify the earthquake interactions worldwide (Stein et al., 1994; Harris, 1998; Nalbant et al., 1998; Shen et al., 2003; Papadimitriou and Sykes, 2001; Papadimitriou et al., 2004, 2007; Liu et al., 2007; Chen et al., 2008; Gkarlaouni et al., 2008; Han et al., 2008; Karakostas et al., 2013), the aftershock distribution (Stein and Lisowski, 1983; King et al., 1994; Deng and Sykes, 1997; He et al., 2013; Chan and Wu, 2014), and the stress change on target faults (Sarkar and Chander, 2003; Parsons et al., 2008; Toda et al., 2008; Wan et al., 2010; He et al., 2011; Li et al., 2013; Qian and Han, 2013). The interaction between large earthquakes may be considered a source of earthquake triggering, and the aftershock distribution may be defined by the Coulomb failure criterion. Aftershocks are plentiful in which the Coulomb failure pressure increases and sparse where the Coulomb failure pressure decreases. Furthermore, the Coulomb failure stress changes have established quite efficient at figuring out the locations of large earthquakes in the surroundings. However, Coulomb failure stress change (ΔCFF) may be clearly expressed as (Freed, 2005; Harris, 1998; King and Cocco, 2000; King et al., 1994; Stein et al., 1994; Toda et al., 1998):

$$\Delta CFF = \Delta\tau + \mu'(\Delta\sigma + \Delta P) \qquad (13)$$

where $\Delta\tau$ is the shear stress change along the slip direction on the assumed fault plane, μ is the coefficient of friction, $\Delta\sigma$ is the normal stress change, and ΔP is the change in pore fluid pressure. Stress changes were computed on receiver planes due to rectangular dislocations in a uniform, elastic half-space with a Poisson's ratio of 0.25 and shear modulus of 3.3×10^4 MPa. However, for a strike-slip fault, μ is commonly considered to be low (e.g., 0.4), whereas for a continental thrust μ is generally higher (up to 0.8) (King et al., 1994). Lower obvious coefficient of friction ought to arise if the fault has encountered more cumulative slip (Parsons et al., 1999). However, μ = 0.4 was used in these stress calculations based on the coseismic elastic dislocation modelling of the earthquakes (Okada, 1992) by assuming earthquake ruptures as rectangular dislocation surfaces in an elastic half-space having Young's modulus of 8×10^5 bar and Poisson's ratio of 0.25. Coulomb 3.3 software was used to calculate Coulomb failure stress changes (Lin and Stein, 2004; Toda et al., 2005).

To understand whether the first main shock changed the proximity to failure on the second main shock fault, the change in the Coulomb stress associated with the first main shock may encourage or discourage the main shock fault was examined. The first main shock of magnitude M_N 6.5 occurred NE of the second main shock epicenter with magnitude M_N 6.0. The NE–SW trending plane is considered as the fault plane of first main shock. The stress changes caused by the first main shock are shown in Fig. 7. The Coulomb stress change due to the first main shock fault (rp1 strike = 36°, dip = 87°, rake = 180°) was calculated on the second main shock receiver fault (rp1strike = 129°, dip = 77°, rake = −5°). At first glance, in Fig. 7, the stress-increased or bright zone can accelerate the seismicity while the stress-shadow zone can decelerate. It is observed that the second main shock epicenter of magnitude M_N 6.0 took place in the lobe of increased (positive) Coulomb stress which shows that second main shock was

promoted to failure due the transfer of positive Coulomb stress by coseismic slip of first main shock and thus triggered by first main shock. The calculated Coulomb stress changes due to first main shock, in a cross-section along line AB passing through the second main shock's epicenter; this shows that the second main shock hypocenter is placed in increased (positive) stress region, evidencing the triggering of second main shock due to first main shock (Fig. 7b). Both the second main shock's epicenter and hypocenter are located in areas of positive or increased Coulomb stress change imparted by either the first main shock on second main shock fault (Fig. 7a and b). By considering apparent friction coefficient as $\mu' = 0.4$ (Fig. 7), the coseismic Coulomb failure stress change on the slip direction of the second main shock increased by 0.866 bar. The stress change exceeded the earthquake triggering threshold of 0.1 bar, implying an apparent triggering effect.

However, both main shocks were followed by a number of aftershocks during the period December 20, 2010–April 6, 2011. The epicentral distribution of the aftershocks suggests that the causative faults of the first main shock is aligned in a NE-SW direction and second main shock is aligned in a NW-SE direction, which were activated during the seismic activity. The coseismic Coulomb stress changes due to the both main shocks were calculated to analyze the correlation between increased Coulomb stress regions and locations of aftershock activity. The computation of Coulomb stress field for depth range 0– 30 km (Fig. 8) was performed for $\mu' = 0.4$. The coseismic Coulomb stress changes were resolved on optimally-oriented planes of strike-slip faults. To see the overall spatial relationship between Coulomb stress change and aftershock distribution, aftershocks were overlain onto the Coulomb stress change fields. Correlation is strong between increased Coulomb stress region and locations of observed aftershocks as more than 90% of the total aftershocks occurred in the increased zone. Most of the Rigan aftershocks

406 occur in enhanced Coulomb stress regions suggesting that these shocks were triggered due to a
407 transfer of positive Coulomb stress by main shocks. Freed (2005) states the best correlation
408 between increased Coulomb stress and locations of aftershocks is observed at distances larger
409 than a few kilometers from the fault rupture. The slip distribution and rupture geometry influence
410 the near-fault stress changes. The occurrence of aftershock activity in stress shadow regions is
411 generally due to over simplifications of modeled fault-slip, unaccounted heterogeneity of crust
412 and existence of small faults with different azimuthal orientations. A few aftershocks occurred in
413 the region of decreased Coulomb stress (stress shadow region; Fig. 8). Ideally a few aftershocks
414 or triggered earthquakes should occur in such regions if the Coulomb hypothesis is valid (Harris
415 and Simpson, 1998).

416 ## 6. **Results and Conclusion**

417

418 Recent years have demonstrated a noteworthy consideration paid to aftershock sequences,
419 since they can help in understanding the mechanism of earthquakes and they are useful
420 resources of data about earthquakes nucleation and the physical properties of materials in
421 fault areas in which slip takes place during an earthquake (Frohlich and Willemann, 1987).
422 Kisslinger and Jones (1991) and Kisslinger (1996) recommended that large amounts of
423 residual seismic energy is generated by heterogeneous materials in the focal region
424 considered is discharged by aftershocks. Statistical properties of aftershocks have been
425 studied for long time (Utsu, 1961, 1969; Utsu et al., 1995; Guo and Ogata, 1999). However,
426 most studies managed only to assess the distribution of aftershocks in time, space and
427 magnitude domains. For this work, aftershock data from IGUT's earthquake catalog the
428 period December 20, 2010 till April 6, 2011 was adopted. Two main aftershock sequences

which triggered by two main shocks during the Rigan sequence have been considered; the first sequence which was triggered by an event on December 20, 2010 with magnitude M_N 6.5 and second sequence which triggered by separate event which occurred on January 27, 2011 with magnitude M_N 6.0. The causative fault related with the first and second sequence has a NE–SW and NW-SE strike respectively, as documented by both, spatial aftershock distribution and fault plane solution determined.

The *b*-value of the Gutenberg–Richter frequency magnitude was estimated using the maximum likelihood estimation. To derive dependable *b*-value estimates, only events with magnitude over the threshold magnitude of completeness M_c were chosen. The magnitude above which the total events have been recorded, M_c, is a critical parameter for seismicity-based investigations since it is important to utilize the maximum number of events to determine such seismic hazard values, which drives regularly to underestimation of M_c (Wiemer and Wyss, 2000). As shown in Fig. 4, M_c was equal to 3.2 for both sequences, and the *b*-value was calculated equal to b = 0.89±0.08 and b = 0.88±0.08 for the first sequence and second sequence respectively. The processed *b*-values are smaller than the worldwide mean estimation of 1.0 which is associated with a low degree of heterogeneity, large velocity of deformation and large faults (Manakou and Tsapanos, 2000). The low *b*-value is additionally synonymous to the occurrence of larger size aftershocks that are affected because of the attendance of giant size asperities in the rupture zone. The estimated low *b*-value for these main shocks sequences drives that the region is indicated by large differential stress and the genesis of giant aftershock activity in a short time interval gives power this.

The significant change among the magnitudes of the main shock and the biggest aftershock relies on the stress situation and heterogeneity of the rock mass. Based on Bath's law

(Bath, 1965), the distinction between the size of the main shock and the biggest aftershock of an earthquake sequence has a steady statistical mean value of 1.2, and is outwardly independent of the magnitude of the main shock. It infers that the strain transfer chargeable for the incidence of aftershocks is a self-similar process (Shcherbakov and Turcotte, 2004). However, the relationship among magnitude of the main shock and its biggest aftershock for both sequences has been studied on the basis of modified Bath's law. The magnitude difference (Δm) is found to be 1.4 and 0.7 for first and second sequence respectively. So that both sequences do not pursue the Bath's law. Similar characteristics are also reported by many previous authors (e.g Papazachos et al., 1967; Shcherbakov et al., 2005; Hamdache et al. , 2013). Taking after Shcherbakov and Turcotte (2004), Bath's law and the Gutenberg–Richter relationship are consolidated keeping in mind the end goal of determining the biggest aftershocks (m^*) which can happen in each sequence. This m^* is directly associated to the parameter a and b of the Gutenberg–Richter by the relation $a = bm^*$. The independence of the fraction of the elastic energy which expands the stress in contiguous rock, on the size of earthquake clarifies the legitimacy of Bath law in its unique and modified model (Shcherbakov and Turcotte, 2004). However, Shcherbakov and Turcotte (2004) concluded that all the aftershocks play a similar role in relaxing the stress transferred by the main shock. The partitioning of energy requires that an expansive division of collected energy is discharged in the main shock and just a moderately little part of the energy discharged in the aftershock succession. Therefore, by taking a = 4.77 and b = 0.89 for the first sequence and a = 4.86 and b = 0.88 for the second sequence the modified magnitude of biggest aftershock (M^*) as 5.3 and 5.5 for first and second sequences respectively. Moreover, magnitude differences ($\boldsymbol{\Delta} m^*$) as 1.2 and 0.5 for first and second sequences have been calculated respectively. However, 2.2% of all energy is related with

aftershock activity while 97.8% is associated with main shock in the first sequence. In comparison, 20% of the total energy is associated with aftershock activity while 80% is associated with main shock for the second sequence. In any case, The power content of the aftershock sequence is increasing with lowering Δm.

The temporal decay of aftershocks pattern has been evaluated using the modified Omori law (Utsu et al., 1995). In keeping with Olssen (1999) and Utsu et al. (1995), *p*-values usually range between 0.5 and 1.8, and this parameter differs from sequence to sequence based on tectonic situation in the considered area. However, it is not clear which factor impact most on calculated *p*- values. More consideration is paid in the estimation of the *p*-value utilizing the maximum likelihood as explained by Nyffengger and Frolich (1998, 2000). The *p*-value equal to 1.1 ± 0.12 and 1.1 ± 0.1 were obtained for first and second sequences respectively. The *p*-value is larger than the mean value (1.0) in the both sequence. The higher *p*-value infers faster decay of aftershock activity. However, the *p*-value approaching a value of 1.0 pronounces that earthquake happened in an tectonically active region with an amount of stress dissipation.

A natural way to analyze the spatial distribution of seismicity is to determine the so called fractal dimension (D_c-value). In particular, fault networks and epicenter distributions have fractal properties (Goltz, 1998). It is well identified that earthquakes cluster both in time and space, either on a long-term (Kagan and Jackson, 1991) or in the short-term time scale (foreshocks and aftershocks). For evaluating fractal dimension values, the correlation dimension approach was adopted, which is seen to be a more robust means for point process interrogation. Be that as it may, the variety in fractal measurement zones gives a lot of information about the geological heterogeneity and constancy of the region (Dimitriu et al., 1993; DeRubeis et al., 1993). Moreover, value of D_c near to zero may be interpreted as being all events bunched into

498 one point, near to 1.0 indicates dominance of the sources, near to 2.0 indicates the planar
499 fractures surface being filled up and a value near to 3.0 indicates that earthquake fractures are
500 topping off a crustal volume. In this research, the spatial fractal dimension was evaluated from
501 the double-logarithmic plot of the correlation integral and distance between hypocenters, and
502 found equal to 2.34 ± 0.03 and 2.54 ± 0.02 for the first and second sequences respectively
503 (Fig. 6). A D_c-value higher than 2.0 reveals that the earthquakes are haphazardly distributed in
504 the fault zone crustal volume.

505 There are numerous studies attempting to understand earthquake interactions that have
506 concentrated on the hypothesis of static stress transfer as a possible triggering mechanism.
507 Calculation of static Coulomb strain can assist our understanding to comprehend stress
508 interaction process and to provide an explanation for the evolution of seismicity patterns (e.g.,
509 Harris, 1998; Stein, 1999). The Coulomb stress change due to the first main shock which
510 occurred on December 20, 2010 with magnitude of M_N 6.5 (Global CMT M_w 6.5) was calculated
511 and examined in relation to its probable interaction with the second main shock which occurred
512 on January 27, 2011 with magnitude of M_N 6.0 (Global CMT M_w 6.2). The Coulomb stress
513 change indicates that the epicenter of second main shock located in the positive (increased)
514 Coulomb stress lobe. Moreover, the cross-sectional and map views of the Coulomb stress change
515 due to the first main shock indicates that the second main shock lies in the increased (positive)
516 Coulomb stress lobe. Moreover, the second main shock was calculated to receive approximately
517 0.866 bar. It is clear that the Coulomb stress change surpassed the triggering threshold of 0.1 bar
518 which reveals that the second main shock was triggered by the transfer of positive Coulomb
519 stress due to a first main shock. coseismic Coulomb stress modeling was performed for both
520 main shocks. The assemblage between aftershock distribution and increased Coulomb stress

521 region indicates that more than 90% aftershocks have been triggered by transfer of positive
522 Coulomb stress due to coseismic slip of these main shocks. The correspondence between
523 aftershock activity and the positive Coulomb failure stress regions produced by these main
524 shocks are in good agreement with previous studies that provide a possible explanation of
525 aftershock triggering in this situation (King et al., 1994; Stein et al., 1994; Harris, 1998; Toda et
526 al., 1998; Karakostas et al., 2003, 2004; Rajput et al., 2005; Gahalaut, 2008; Bayrak et al., 2013).
527

528 **Acknowledgments**

529 The authors would like to thank the Institute of Geophysics at University of Tehran (IGUT) for
530 providing their data for analysis. The Computer programs, Coulomb 3.3 (Toda et al. 2011) and
531 Zmap (Wiemer, 2001) were also used.
532

533 **References**

534 Ambraseys, N N., Melville, C P., 1982. A History of Persian Earthquakes, Cambridge University
535 Press, Cambridge.

536 Ashtari-Jafari, M,. 2011. Teleseismic source parameters of the Rigan county earthquakes and
537 evidence for a new earthquake fault, Pure Appl. Geophys. 169, 1655–1661, doi:
538 10.1007/s00024-011-0433-9.
539

540 Bayrak, Y.,, Yadav, R B S., Kalafat, D., Tsapanos, T M., Çınar, H., Singh, A P,. Bayrak, E,.
541 Yılmaz, Ş., Öcal, F., Koravos, G., 2013. Seismogenesis and earthquake triggering during
542 the Van (Turkey) 2011 seismic sequence. Tectonophysics, 601 (2013) 163–176.
543

544 Bath, M., 1965. Lateral inhomogeneties in the upper mantle. Tectonophysics 2, 483– 514.

545

546 Ben-Zion, Y., 2008. Collective behavior of earthquakes and faults: Continuum-discrete
547 transitions, progressive evolutionary changes, and different dynamic regimes. Rev
548 Geophys 46: RG4006.i:10.1029/2008rg000260.

549

550 Berberian, M., 1976. Contribution to the Seismotectonics of Iran (Part II)". Geological Survey of
551 Iran, Report No. 39, p. 517.

552

553 Berberian, M., 1995. Natural hazards and the first earthquake catalogue of Iran, historical
554 hazards in Iran prior to 1900. A UNESCO/IIEES Publication During UN/ IDNDR IIEES,
555 Iran.

556

557 Bowman, J. R., 1997. A seismicity precursor to a sequence of Ms 6.3-6.7 midplate earthquakes
558 in Australia, Pure Appl. Geophys., *149*, 61-78.

559

560 Chan, C H., Wu, Y M., 2014. Seismic behavior in central Taiwan: response to stress evolution
561 following the 1999 Mw 7.6 Chi-Chi earthquake. J. Asian Earth Sci. 90, 101–105.

562

563 Chen, L W., Zhang, P Z., Lu,Y Z., 2008. Numerical simulation of loading/ uploading effect on
564 Coulomb Failure stress among strong earthquakes in Sichuan-Yunnan area. Chin. J.
565 Geophys. 51 (5), 1411–1421.

566

Console, R., Lombardi, A M., Murru, M., Rhodes, R., 2003. Bath's law and the selfsimilarity. J. Geophys. Res. 108, 2128.

Deng, J., Sykes, L R., 1997. Evolution of the stress field in Southern California and triggering of moderate-size earthquakes: a 200-year perspective. J. Geophys. Res. 102 (B5), 9859–9886.

DeRubeis, V., Dimitriu, P., Papadimitriou, E., Tosi, P., 1993. Recurrent patterns in the spatial behavior of Italian seismicity revealed by the fractal approach. Geophys Res Letts 20/18, 1911–1914.

Dimitriu, P P., Papadimitriou, E E., Papazachos, B C., Tsapanos, T M., 1993. Global study of the distribution of earthquakes in space and in time by the fractal method. In: Proc. 2nd Cong. Hellenic Geophys. Union, Florina, May 5–8, 1993, vol. 1, pp. 164–174.

Freed, AM., 2005. Earthquake triggering by static, dynamic, and postseismic stress transfer. Ann Rev Earth and Planetary Sci 33, 335–367.

Frohlich, C., Willemann , R., 1987 .Statistical methods for comparing directions to the orientations of focal mechanisms and wadati-beniof zones. Bull. Seismol. Soc. Am. 77 (6), 2135–2142.

589 Gahalaut, V K., 2008. Coulomb stress change due to 2005 Kashmir earthquake and implications
590 for future seismic hazards. J Seismol 12, 387–394.
591
592
593 Gkarlaouni, Ch., Papadimitriou, E E., Karakostas, V G., 2008. Implication of fault interaction to
594 seismic hazard assessment in Sichuan-Yunnan provinces of southeastern China. Acta
595 Seismol. Sin. 21 (2), 181–201.
596
597 Goltz, C., 1998. Fractal and chaotic properties of earthquake, in Lecture Notes in Earth Sciences,
598 Springer, New York, 175 pp.
599
600 Grassberger, P., Procaccia, I., 1983. Measuring the strangeness of strange attractors. Physics D 9,
601 189–208.
602
603 Guo, Z., Ogata, Y., 1999. Statistical relation between the parameters of aftershocks in time,
604 space and magnitude. J. Gophys. Res. 102 (B2), 2857–2873.
605
606 Gutenberg, B., Richter, C.F., 1944. Frequency of earthquakes in California. Bulletin of the
607 Seismological Society of America 34, 185–188.
608
609 Hamdache, M., Pelaez, J A., Talbi, A., 2013. Analysis of aftershock sequences in South and
610 Southeastern Spain. Phyics and Chemist of the Earth 63 (2013) 55–76.
611

612 Han, Z J., Dong, S P., Xie, F R., 2008. Earthquake triggering by static stress: the 5 major
613 earthquakes with MP7 (1561–1920) in the northern section of south– north seismic zone,
614 China. Chin. J. Geophys. 51 (6), 1776–1784.
615
616 Hardebeck, J L., Nazareth, J J., Hauksson, E., 1998. The static stress change triggering model:
617 Constraints from two southern California aftershocks sequences. J Geophys Res. 103,
618 24,427–24,437.
619
620 Harris, R A., 1998. Introduction to special section: stress triggers, stress shadows and
621 implications for seismic hazard. J Geophys Res 103 (10), 24347–24358.
622
623 Harris, R., Simpson, RW., 1988. Suppression of large earthquakes by stress shadows: a
624 comparison of Coulomb and rate-state failure. J Geophys Res 103:24439–24451.
625
626 He, J K., Xia ,W H., Lu, S J., 2011. Three-dimensional finite element modeling of stress
627 evolution around the Xiaojiang fault system in the southeastern Tibetan plateau during
628 the past _500 years. Tectonophysics 507, 70–85.
629
630 He, P., Wen, Y M., Xu, C J., 2013. The large aftershocks triggered by the 2011 Mw9.0 Tohoku-
631 Oki earthquake, Japan. J. Asian Earth Sci. 74, 1–10.
632
633 Hessami, KH., Jamali, F., 2006. Explanatory notes to the map of major active faults of Iran. J
634 Seismol Earthq Eng 8(1):1–11.

635 Hirata, T., 1989. A correlation between the b-value and the fractal dimension of earthquakes. J.
636 Geophys. Res. 94, 7507–7514.
637
638 Kagan, Y Y., Jackson, D D., 1991. Long term earthquake clustering: J Geophys Res , 104, 117-
639 133.
640
641 Karakostas, V G., Papadimitriou, E E., Karakaisis, G F., Papazachos, C B., Scordilis, E M.,
642 Vargemezis, G., Aidona., E., 2003. The 2001 Skyros, Northern Aegean, Greece,
643 earthquake sequence: off-fault aftershocks, tectonic implications and seismicity
644 triggering. Geophys Res Letts, Vol 30, Issue 1, Pages 12-1–12-4.
645
646 Karakostas, V G., Papadimitriou, E E., Papazachos, C B., 2004. Properties of the 2003 Lefkada
647 Ionian Islands, Greece, earthquake seismic sequence and seismicity triggering. Bull
648 Seismol Soc Am 94, 1976–1981.
649
650 Karakostas, V., Papadimitriou, E., Jin, X S,. 2013. Potential of future seismogenesis in Hebei
651 Province (NE China) due to stress interactions between strong earthquakes. J. Asian
652 Earth Sci. 75, 1–12.
653
654 King, G.C.P., Cocco, M., 2000. Fault interactions by elastic stress changes: new clues from
655 earthquake sequences. Advances in Geophysics 44, 1–38.
656

King, G C P., Stein, R S., Lin, J., 1994. Static stress changes and the triggering of earthquakes. Bull Seismol Soc Am 84, 935–993.

Kisslinger, C., Jones, L M., 1991. Proprieties of aftershocks in Southern California. J. Geophys. Res. 103 (24), 453-24,465.

Kisslinger, C., 1996. Aftershocks and fault-zone properties. Adv. Geophys. 18, 1–36.

Kisslinger, C., Jones, L. M., 1991. Proprieties of aftershocks in Southern California. J. Geophys. Res. 103 (24), 453-24,465.

Li, Y J., Chen, L W., Lu, Y Z., 2013. Numerical simulation on influences of Wenchuan earthquake on the stability of faults in the neighborhood. Earth Sci. 38 (2), 398–410.

Lin, J., Stein, R S., 2004. Stress triggering in thrust and subduction earthquakes and stress interaction between the southern San Andreas and nearby thrust and strike-slip faults, J. Geophys. Res., 109, B02303.

Liu. M., Yang, Y., Shen, Z K., 2007. Active Tectonics and Intracontinental Earthquakes in China: The Kinematics and Geodynamics. Geological Society of America, Special Paper 425, pp. 299–318.

679 Manakou, M V., Tsapanos, T M. 2000. Seismicity and seismic hazard parameters evaluation in
680 the island of Crete and the surrounding area inferred from mixed data files,
681 Tectonophysics. 321: 157–178.
682
683 Mendoza, C., Hartzell, S H., 1988). Aftershock patterns and main shock faulting. Bull. Seismol
684 Soc Am. 78, 1438-1449.
685
686 Meyer, B., LeDortz K., 2007. Strike-slip kinematics in Central and Eastern Iran: estimating fault
687 slip-rates averaged over the Holocene, Tectonics, Vol 26, Issue 5.
688
689 Nalbant, S S., Hubert. A., King, G C P., 1998. Stress coupling between earthquakes in northwest
690 Turkey and the north Aegean Sea. J Geophys Res 103, 24,469–24,486.
691
692 Narteau, C., Byrdina, S., Shebalin, P., Schorlemmer, D,. 2009. Common dependence on stress
693 for the two fundamental laws of statistical seismology. Nature, 462/3 December 2009.
694
695 Nuttli, O W., 1973. Seismic wave attenuation relations for eastern North America. J Geophys
696 Res 78, 855–876.
697
698 Nyffengger, P., Frolich, C., 1998. Recommandations for determining p values for aftershock
699 sequence and catalogs. Bull. Seismol. Soc. Am. 88 (5), 1144–1154.
700

Nyffengger, P., Frolich, C., 2000. Aftershock occurrence rate decay properties for intermediate and deep earthquake sequences. Geophys. Res. Lett. 27 (8), 1215– 1218.

Ogata, Y., Imoto, M., Katsura, K., 1991. 3-D spatial variation of b-values of magnitude–frequency distribution beneath the Kanto District, Japan. Geophys. J. Int. 104 (1), 135–146.

Ogata, Y., Katsura, K., 1993. Analysis of temporal and spatial heterogeneity of magnitude frequency distribution inferred from earthquake catalogs, Geophys. J. Int., 113, 727–738.

Okada, Y., 1992. Internal deformation due to shear and tensile faults in a half-space. Bull Seismol Soc Am 82, 1018–1040.

Olssen, R., 1999. An estimation of the maximum b values in the Gutenberg–Richter relation. Geodynamics 27, 547–552.

Papazachos, B C., Delibasis, N., Liapis, N., Moumoulidis, G., Purcaru, G., 1967. Aftershock sequences of some large earthquakes in the region of Greece. Ann. Geofis. 20, 1–93.

Papadimitriou, E E., Sykes, L R., 2001. Evolution of stress field in the Northern Aegean Sea (Greece). Geophys J Int 146, 747–759.

723 Papadimitriou, E E., Wen, X Z., Karakostas, V G., 2004. Earthquake triggering along the
724 Xianshuihe fault zone of western Sichuan, China. Pure Appl Geophys.161, 1683–1707.
725
726 Papadimitriou, E. E., Garlaouni, Ch. G, Jin, X S., 2007. Application of the stress evolutionary
727 model along the Xiaojiang fault zone in Yunnan Province, Southeast China. Acta
728 Geophys. 55 (4), 577–593.
729
730 Parsons, T., Stein, R S., Simpson, R W., 1999. Stress sensitivity of fault seismicity: a comparison
731 between limited-offset oblique and major strike-slip faults. J Geophys Res 104, 20,183–
732 20,202.
733
734 Parsons, T., Chen, J., Kirby, E., 2008 Stress changes from the 2008 Wenchuan earthquake and
735 increase hazard in the Sichuan basin. Nature 454, 509–510.
736
737 Qian, Q., Han, Z J., 2013. Influence of the 2008 Wenchuan earthquake (Mw7.9) on the
738 occurrence probability of future earthquakes on neighboring faults. J. Asia Earth Sci. 70–
739 71, 283–294.
740
741 Rajput, S., Gahalaut,. Sahu, V K ., 2005. Coulomb stress changes and aftershocks of recent
742 Indian earthquakes. Current Science 88 (6), 576–588.
743
744 Rezapour, M., Mohsenpur, A., 2013. The 2010 Mw 6.5 Rigan, Iran, Earthquake Aftershock
745 Sequence, Bull Seismological Soc Am, Vol. 103, No. 3, pp. 1793‑1800.

Rybicki, K., 1973. Analysis of aftershocks on the basis of dislocation theory, Phys. Earth Planet. Inter. 7, 409-422.

Sarkar, I., Chander, R., 2003. Role of static stress transfer in earthquake occurrence in the Himalaya. J. Asian Earth Sci. 22 (1), 59–65.

Scholz, C., 1968. Microfracturing and the inelastic deformation of rock in compression. J. Geophys. Res. 73 (4), 1417–1432.

Schorlemmer, D., Wiemer, S., Wyss, M., 2005. Variations in earthquake-size distribution across different stress regimes. Nature 437 (7058), 539–542.

Shcherbakov, R., Turcotte, D L., 2004. A modified form of Bath's law. Bull. Seismol. Soc. Am. 94, 1968–1975.

Shcherbakov, R., Turcotte, D L., Rundle, J E., 2005. Aftershocks statistics. Pure Appl. Geophys. 162, 1051–1076.

Shen, Z K., Wan, Y G., Gan, W J. 2003. Viscoelastic triggering among large earthquakes along the eastern Kunlun fault system. Chinese J Geophys 46 (6), 786–795.

Stein. R S., 1999. The role of stress transfer in earthquake occurrence. Nature 402, 605–609

769 Stein, R S., Lisowski, M., 1983. The 1979 Homestead Valley earthquake sequence, California:
770 control of aftershocks and postseismic deformation. J. Geophys. Res. Volume 88, Issue
771 Pages 6477–6490.
772
773 Stein, R S., King, G C P., Lin, J., 1994. Stress triggering of the 1994 M=6.7 Northridge,
774 California, earthquake by its predecessors. Science 265 (5177), 1432–1435.
775
776 Stein, S., Wysession, M., 2002. An Introduction to Seismology, Earthquakes and Earth Structure.
777 Blackwell Publishing Press, UK.
778
779 Toda, S., Stein, R S., Reasenberg, P A., Dieterich, J H., 1998 Stress transferred by the Mw = 6.5
780 Kobe, Japan, shock: effect on aftershocks and future earthquake probabilities. J Geophys
781 Res, Volume 103, Issue 10.
782
783 Toda, S., Stein, R., Richards-Dinger, K., Bozkurt, S., 2005. Forecasting the evolution of
784 seismicity in southern California: Animations built on earthquake stress transfer, J.
785 Geophys. Res., Volume 110, Issue 5.
786
787 Toda, S., Lin, J., Meghraoui, M., 2008. 12 May 2008 M = 7.9 Wenchuan, China, earthquake
788 calculated to increase failure stress and seismicity rate on three major fault systems.
789 Geophys. Res. Lett. Volume 35, Issue 17.
790

Toda, S., Stein, R S., Sevilgen, V., Lin, J., 2011. Coulomb 3.3 graphicrich deformation and stress-change software for earthquake, tectonic, and volcano research and teaching-user guide. U.S. Geological Survey Open-File Report 2011-1060.

Turcotte, D., 1997. Fractals and Chaos in Geology and Geophysics. Cambridge University Press, New York, 416 pp.

Urbancic, T., Trifu, C., Long, J., Young, R., 1992. Space–time correlations of b values with stress release. Pure Appl. Geophys. 139 (3), 449–462.

Utsu, T., 1961. A statistical study on the occurrence of aftershocks. Geophysics 30, 521–605.

Utsu, T., 1965. A method for determining the value of b in a formula logN = a – bM showing the magnitude frequency for earthquakes. Geophysical Bulletin Hokkaido University 13, 99–103.

Utsu, T., 1969. Aftershocks and earhquake statistics (I) – some parameters which characterize an Aftershock Sequence and their Interaction. J. Fac. Sci. Hokaido, Univ. Ser. VII (Geophys.) 3, 129–195.

Utsu, T., 2002. A statistical study of occurrence of aftershocks. Geophys. Mag. 30, 521–605.

Utsu, T., Ogata, Y., Matsöra, R S., 1995. The centenary of the Omori formula for a decay law of aftershock activity. J. Phys. Earth 43, 1–33.

Vere-Jones, D., 1969. A note on the statistical interpretation of Bath's law. Bull. Seismol. Soc. Am. 69 (4), 1535–1541.

Vere-Jones, D., Murakami, J., Christophersen, A., 2005. A further note on Bath's law. In: The 4th International Workshop on Statistical Seismology, Tokyo, Japan.

Walker, R T., 2006. A remote sensing study of active folding and faulting in southern Kerman province, S.E. Iran. J. of Struct.Geol., 28, 654–668

Walker, R., Jackson, J. 2004. Active tectonics and late Cenozoic strain distribution in central and eastern Iran, Tectonics, 23, Volume 23, Issue 5 October 2004.

Walker, R T., Bergman, E A., Elliott, J R., Fielding, E J., Ghods, A R., Gorashi, M., Jackson, J., Nazari, H., Nemati, M., Oveisi, B., 2013. The 2010–2011 south Rigan (Baluchestan) earthquake sequence and its implications for distributed deformation and earthquake hazard in southeast Iran, Geophys. J. Int. 193, 349–374.

Wan, Y G., Shen, Z K., Sheng, S. Z,. 2010. The Mechanical effects of the 2008 Ms7.3 Yutian, Xinjiang earthquake on the neighboring faults and its tectonic origin of normal faulting

mechanism. Chin. J. Geophys. 53 (2), 280–289. Volume 54, Issue 6 November 2011, Pages 757–765.

Wiemer, S., 2001. A software package to analyze seismicity: ZMAP. Seismol Res Letts 72, 373–382.

Wiemer, S., Wyss, M., 2000. Minimum magnitude of completness in earthquake catalogs: Examples from Alaska, the Western United States, and Japan. Bull. Seismol. Soc. Am. 90, 859–869.

Yamakawa, N., 1968. Foreshocks, aftershocks and earthquake swarms (IV) – frequency decrease of aftershocks in its initial and later stages. Papers in Meteorology and Geophysics 19, 109–119.

Figure Captions

Fig.1. Simplified tectonic map of SW Iran (Black Stars show epicenter of main shock which occurred December 20,2010 and January 27, 2011, Blue Stars show instrumental event and Gray Stars show Historical event and major faults adopted from Ashtari-Jafari (2011)).

Fig.2. Epicentral location of Rigan sequence occurred during the period of December 20, 2010–April 6, 2011. (Frist main shock shown by Red Star, Second main shock shown by Yellow Star).

Fig.3a. Cumulative number of earthquakes with $M_N \geq 2.6$. The Red star is the first main shock M_N = 6.5) and Yellow star is second main shock (M_N = 6.0).**Fig.3b.** Plot of magnitude

858 versus time. **Fig.3c.** spatial distribution of events, which occurred from December 20,
859 2010 until before Occurrence second main shock (Blue Stars are events with magnitude
860 $M_N \geq 4.0$. **Fig.3d.** spatial distribution of events which occurred from January 27, 2011 till
861 April 6, 2011 (Green Stars are events with magnitude $M_N \geq 4.0$).

862 **Fig. 4.** Frequency–magnitude distribution of G–R relationship (logN = a–bM). **a**, First main
863 shock sequence. **b**, second main shock sequence.

864 **Fig. 5.** Temporal variations decay of *p*-values for Rigan aftershock sequence. **a**, first main shock
865 sequence. **b**, second main shock sequence.

866 **Fig. 6.** Graph which shows the spatial fractal dimension (D_c) of the aftershocks distribution.
867 Solid circles show the data for which best fit was performed for the computation of D_c-
868 value. **a**, First main shock sequence. **b**, second main shock sequence.

869 **Fig.7a.** Coseismic Coulomb stress changes (in bars) due to first main shock (M_w 6.5) resolved at
870 depth 14.3 km (depth of the second main shock (M_w 6.2)). **Fig.7a.** the cross-sectional
871 view of Coulomb stress due to first main shock (M_w 6.5) along line AB.

872 **Fig.8.** Combined coseismic Coulomb stress changes (in bars) due to the first main shock and
873 second main shock within depth range of 0–30 km. The locations of aftershocks occurred
874 during the period December 20, 2010–April 6, 2011 are shown with green circles. **Fig.**

875

876

Fig.1

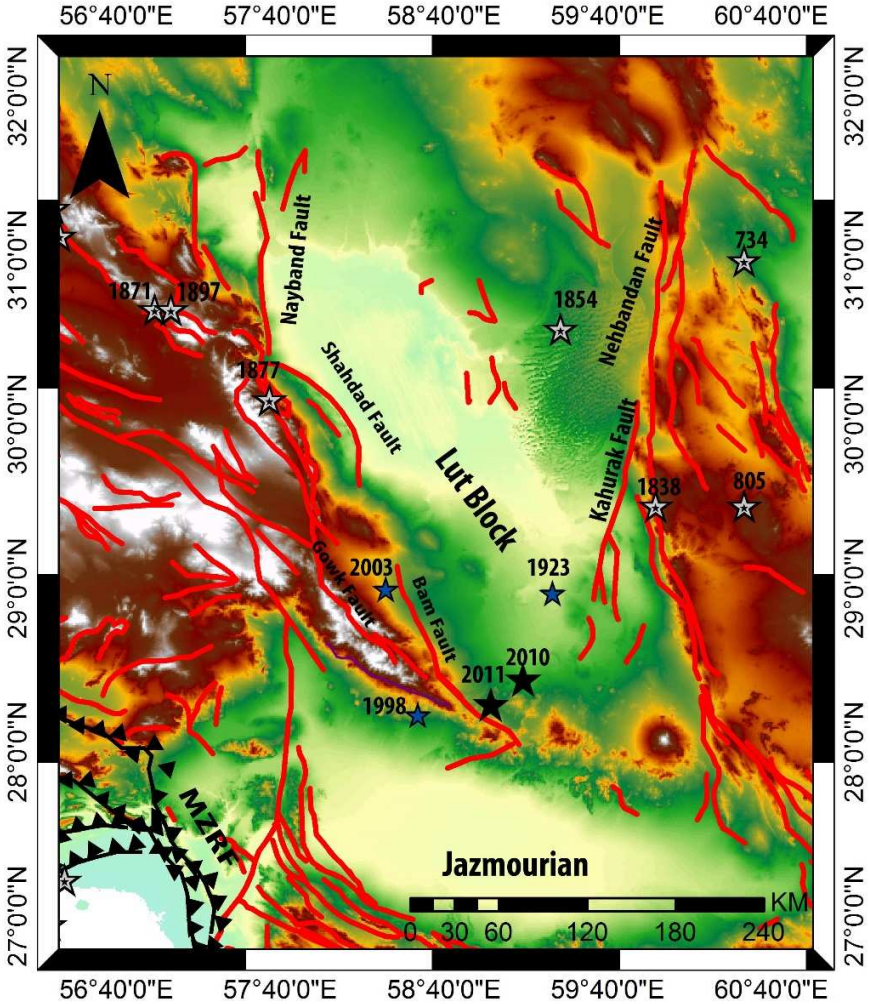

Fig.2

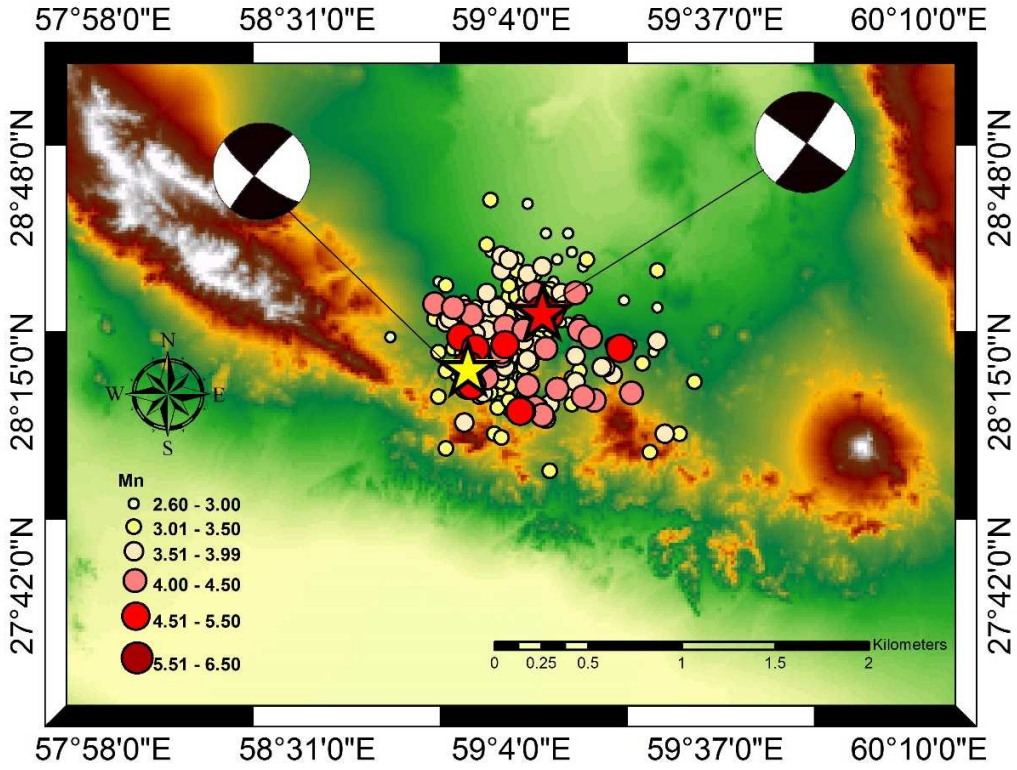

Fig.3.a

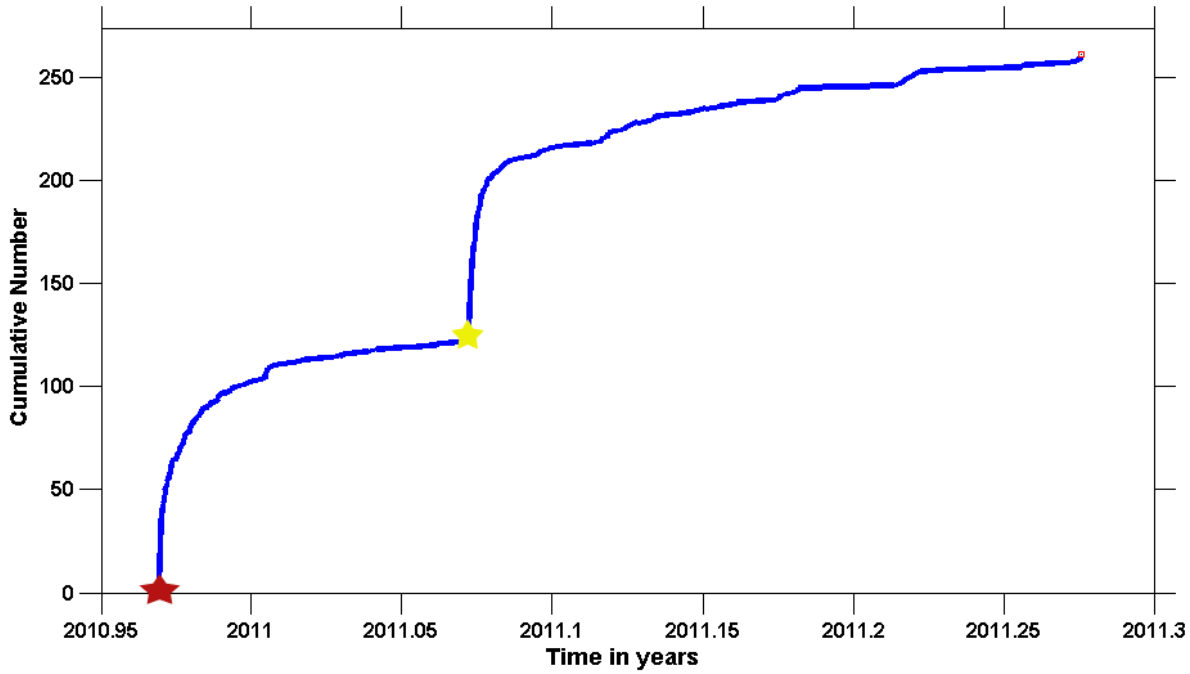
Cumulative Number
250
200
150
100
50
0
2010.95
2011
2011.05
2011.1
2011.15
2011.2
2011.25
2011.3
Time in years

Fig.3.b

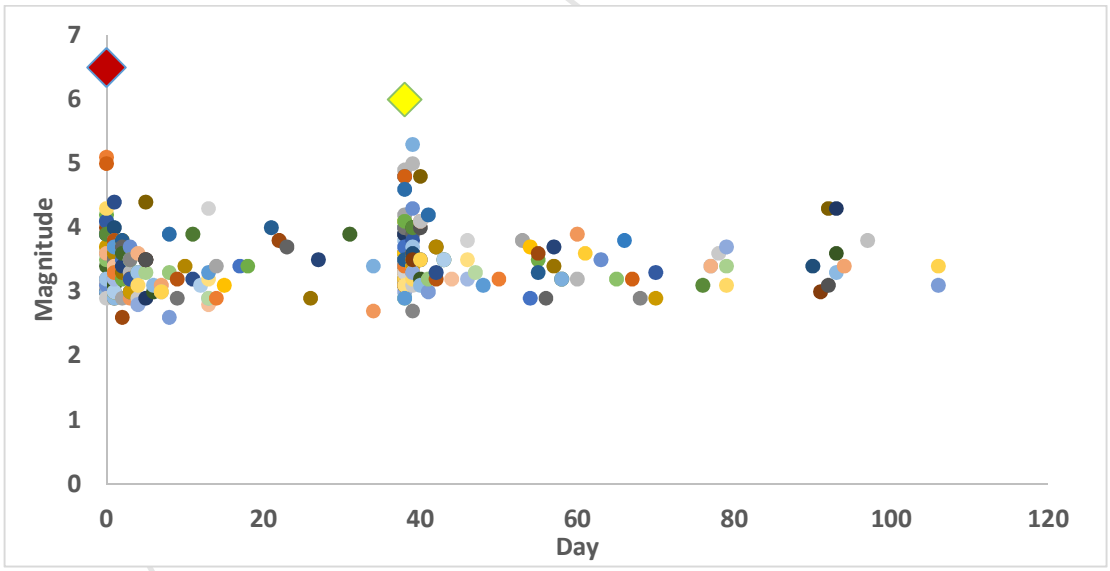
Magnitude
7
6
5
4
3
2
1
0
0
20
40
60
80
100
120
Day

Fig.3c

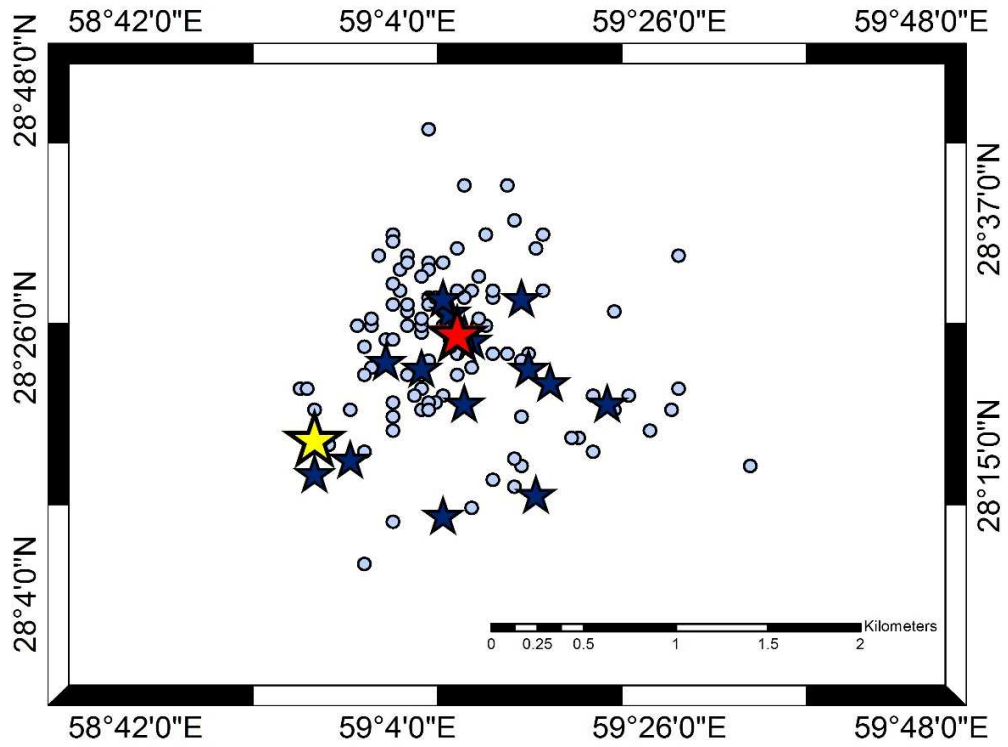
58°42'0"E
59°4'0"E
59°26'0"E
59°48'0"E
28°48'0"N
28°37'0"N
28°26'0"N
28°15'0"N
28°4'0"N
Kilometers
0 0.25 0.5 1 1.5 2

Fig.3d

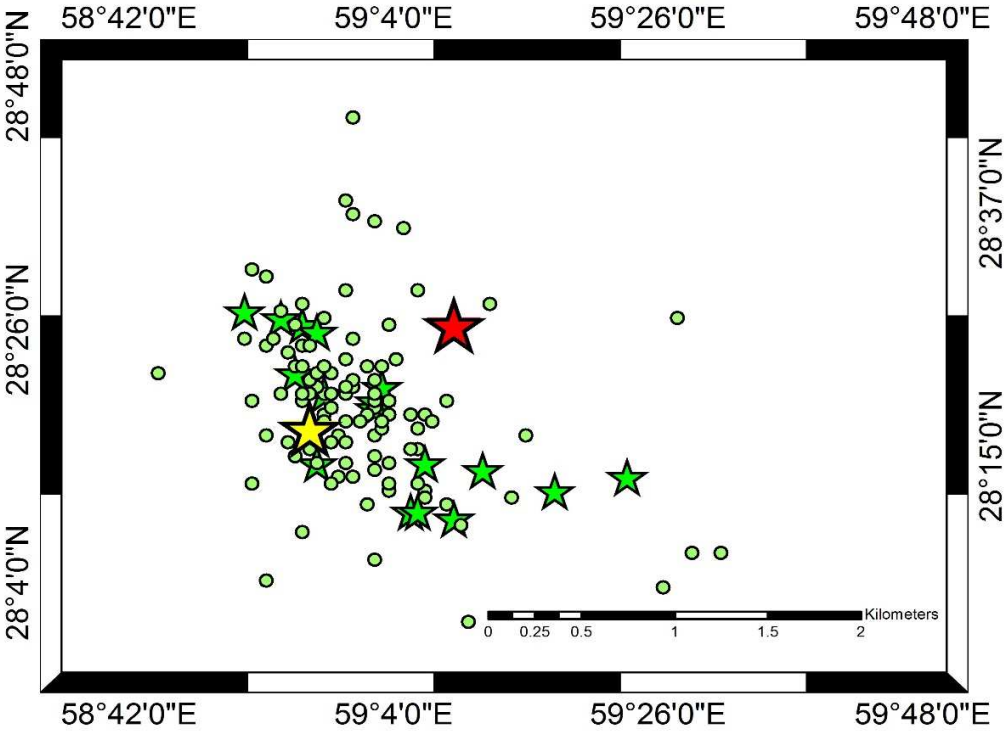
58°42'0"E
59°4'0"E
59°26'0"E
59°48'0"E
28°48'0"N
28°37'0"N
28°26'0"N
28°15'0"N
28°4'0"N
Kilometers
0 0.25 0.5 1 1.5 2

Fig.4a

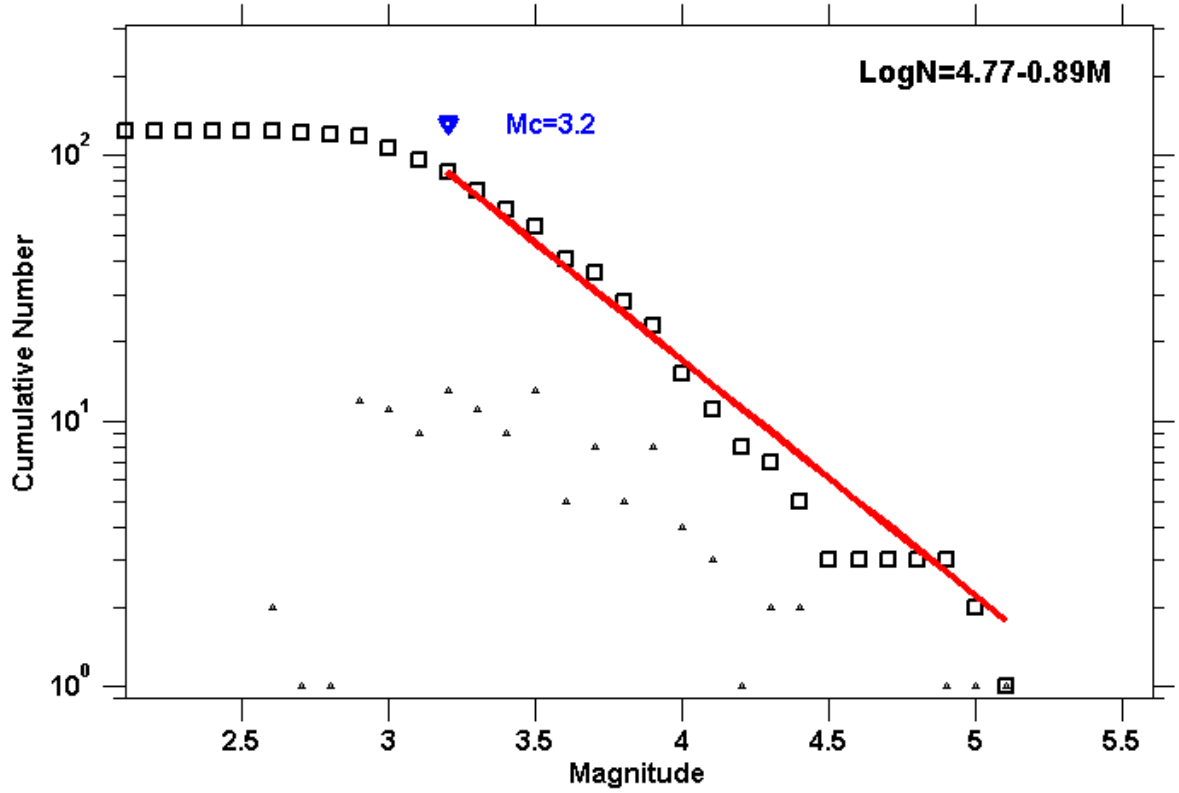

Fig.4b

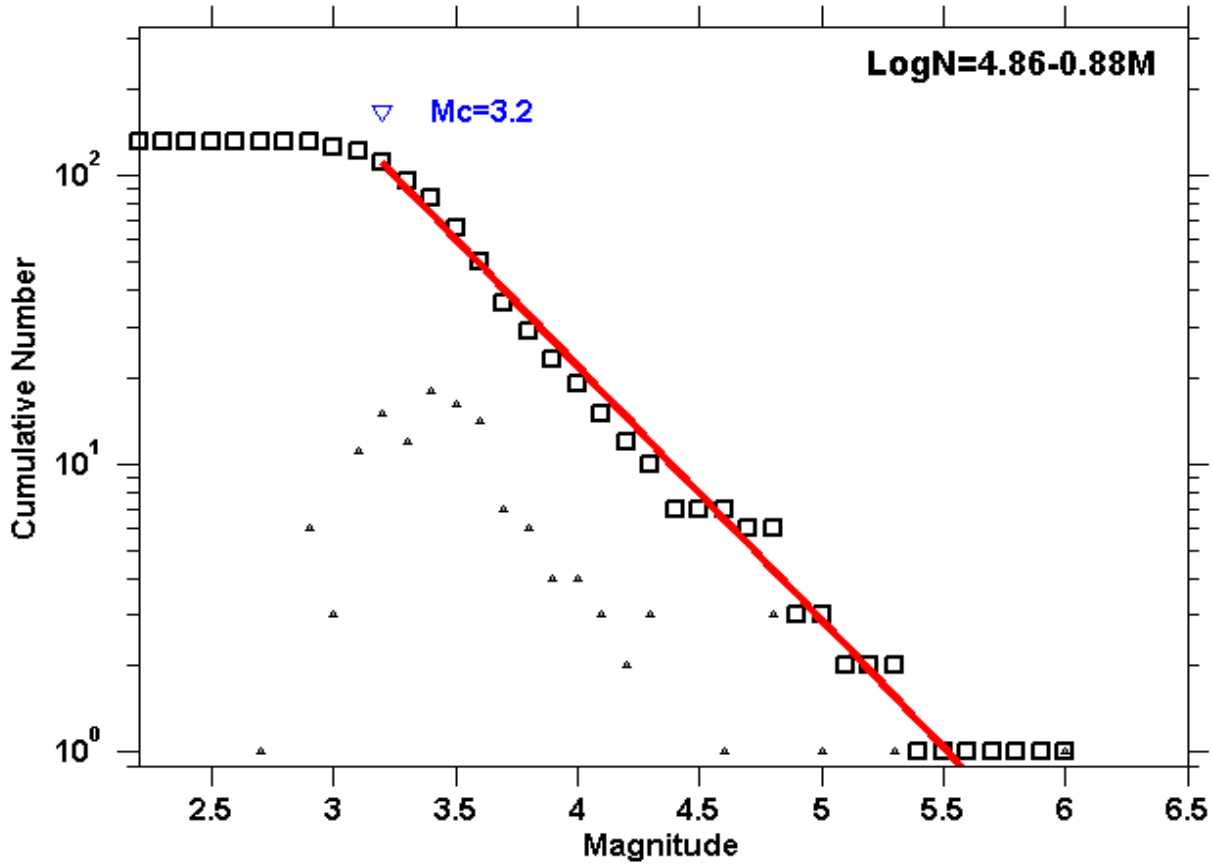

Fig.5a

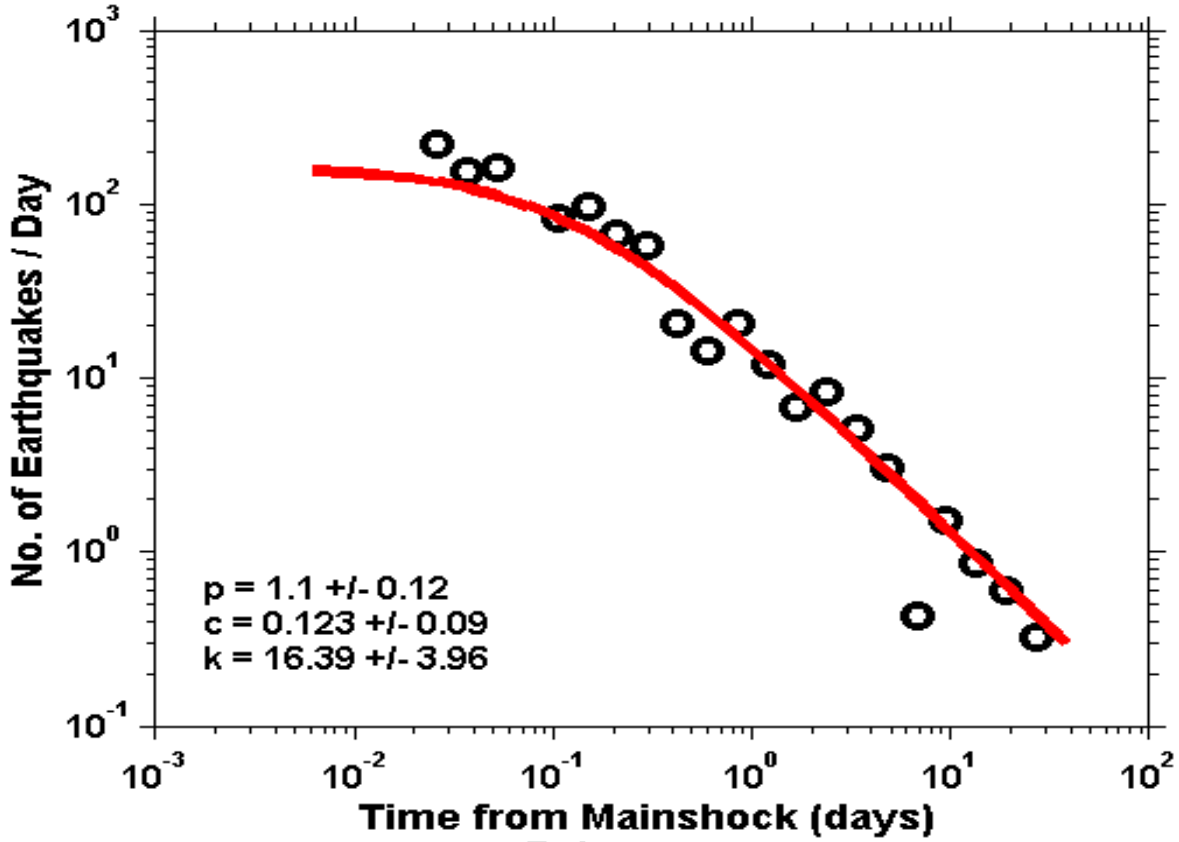

Fig.5b

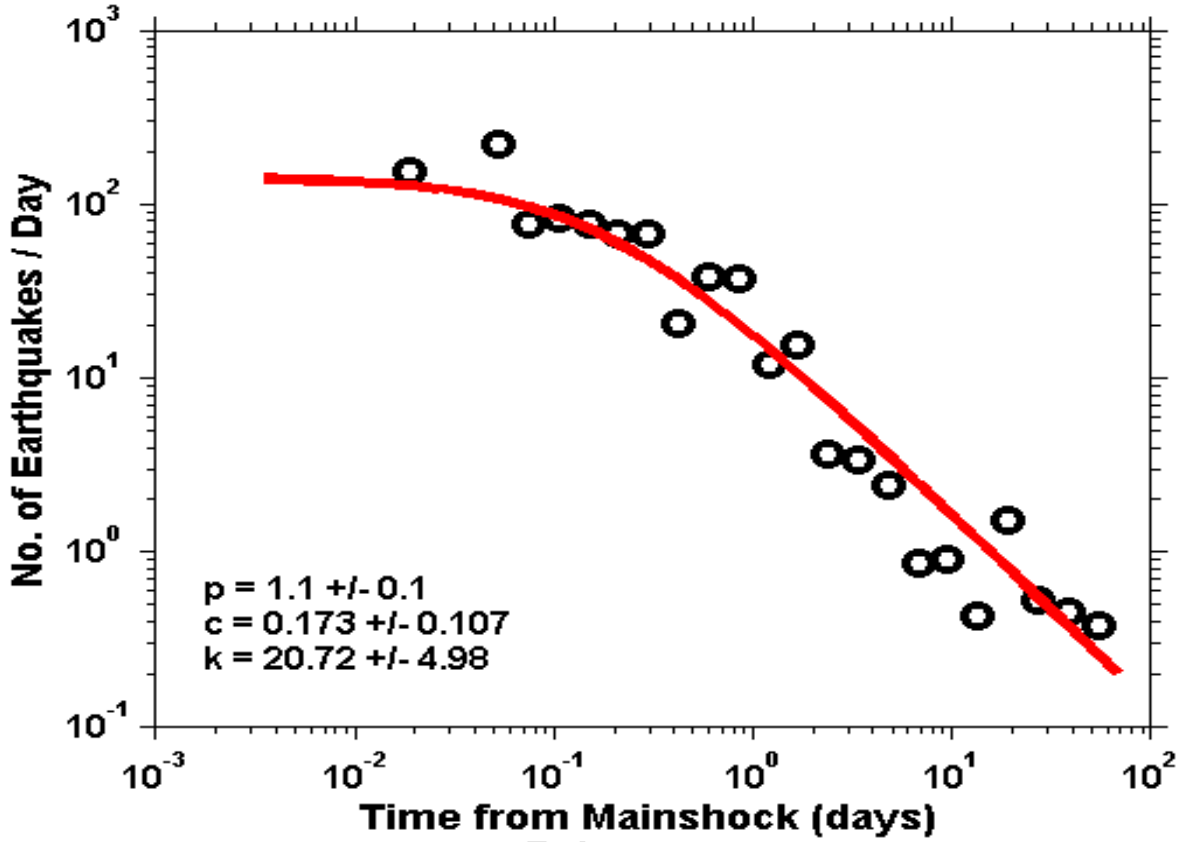

Fig.6a

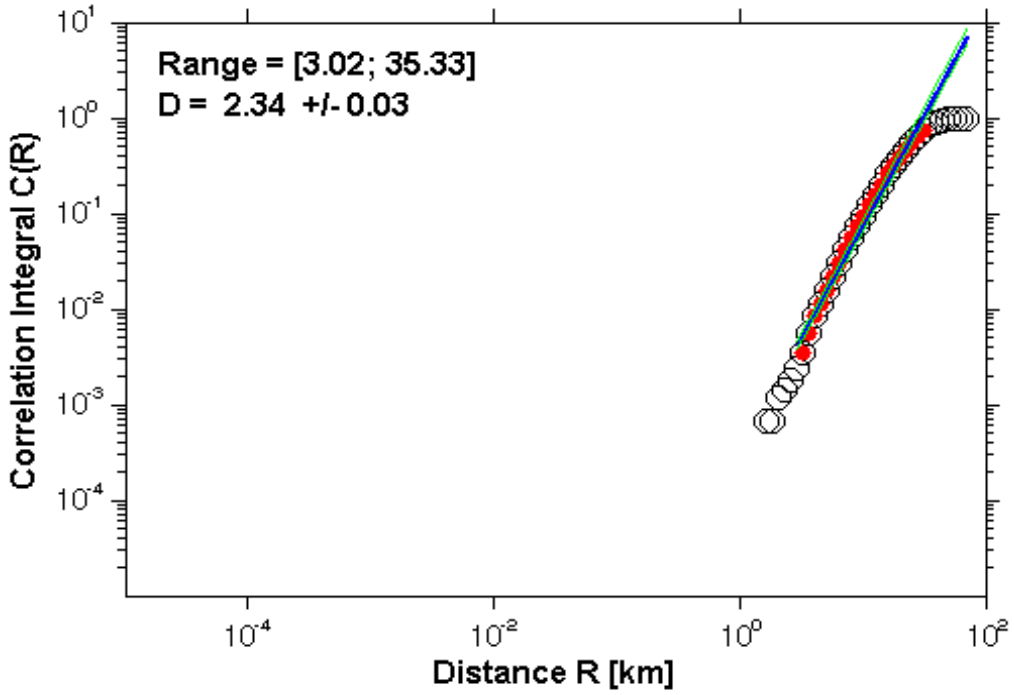
Range = [3.02; 35.33]
D = 2.34 +/- 0.03
Correlation Integral C(R)
Distance R [km]

Fig.6b

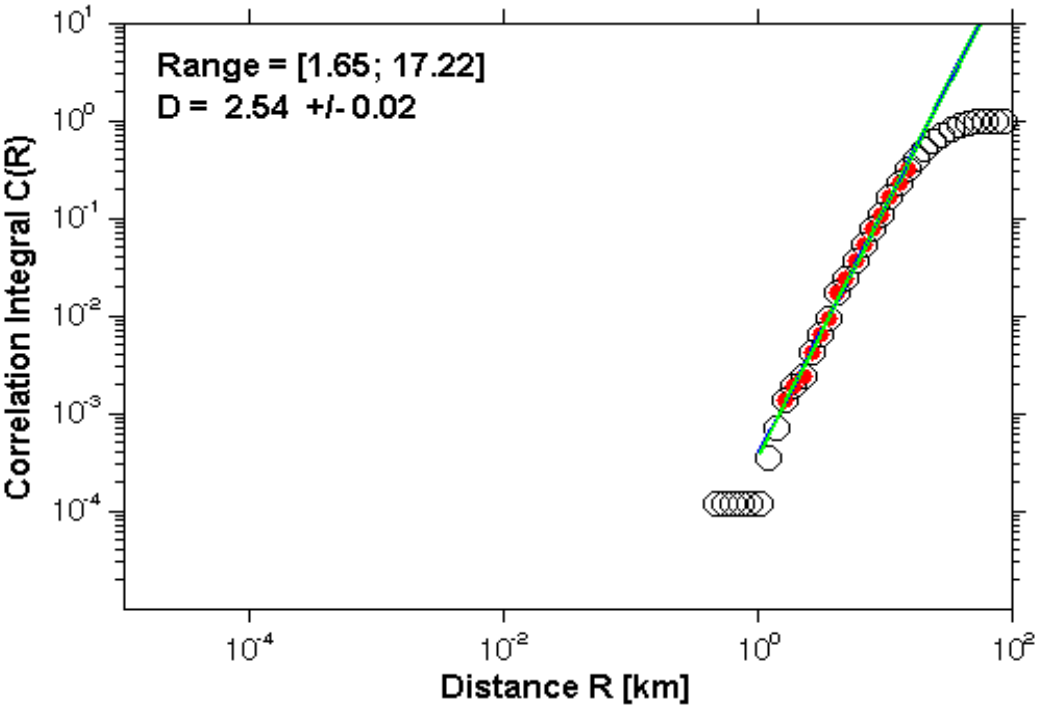
Range = [1.65; 17.22]
D = 2.54 +/- 0.02
Correlation Integral C(R)
Distance R [km]

Fig.7a

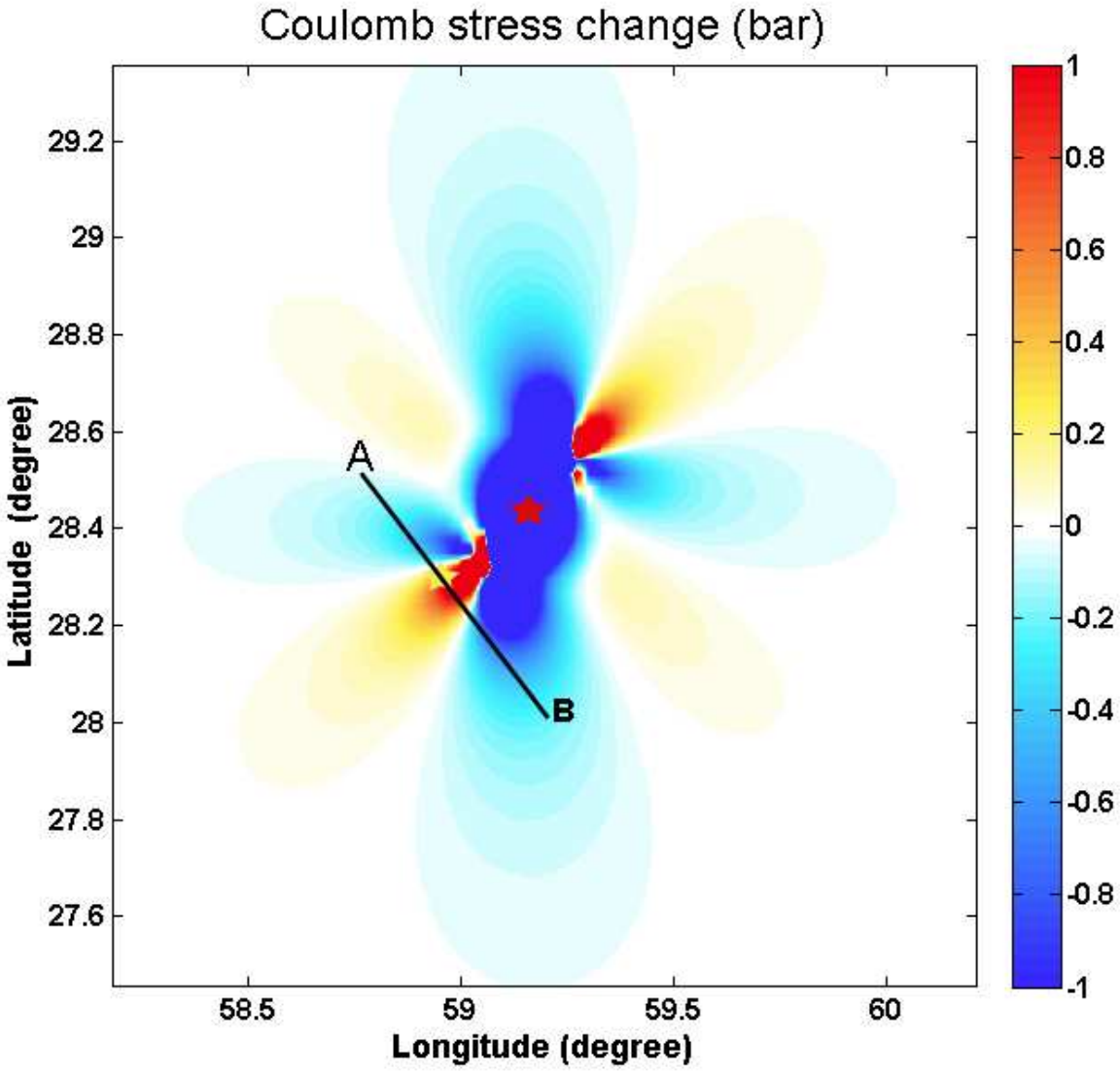
Coulomb stress change (bar)
Latitude (degree)
Longitude (degree)
29.2
29
28.8
28.6
28.4
28.2
28
27.8
27.6
58.5
59
59.5
60
A
B
1
0.8
0.6
0.4
0.2
0
-0.2
-0.4
-0.6
-0.8
-1

Fig.7b

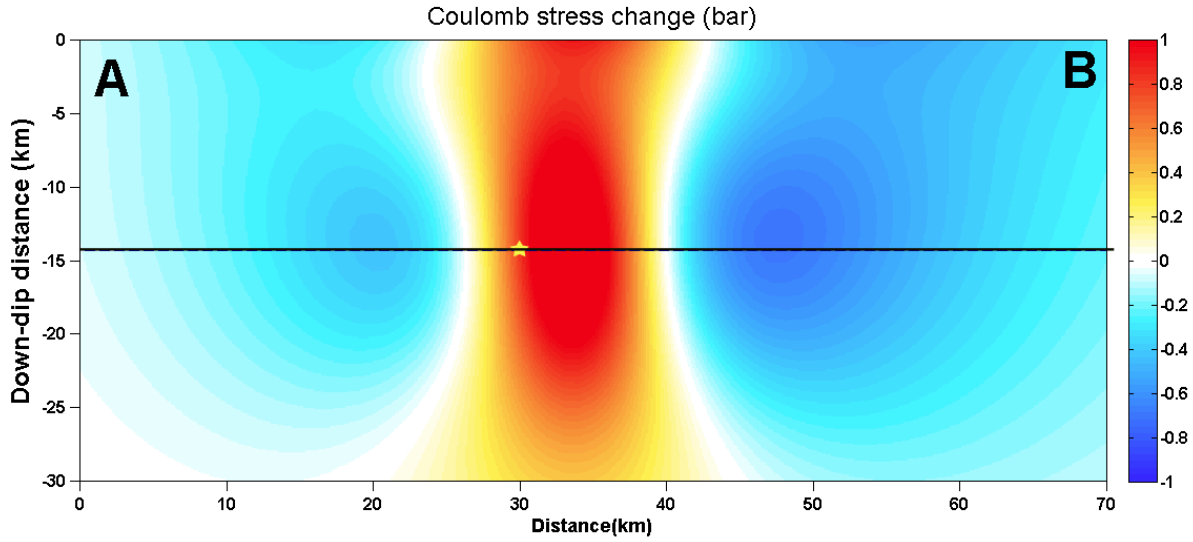

Fig.8

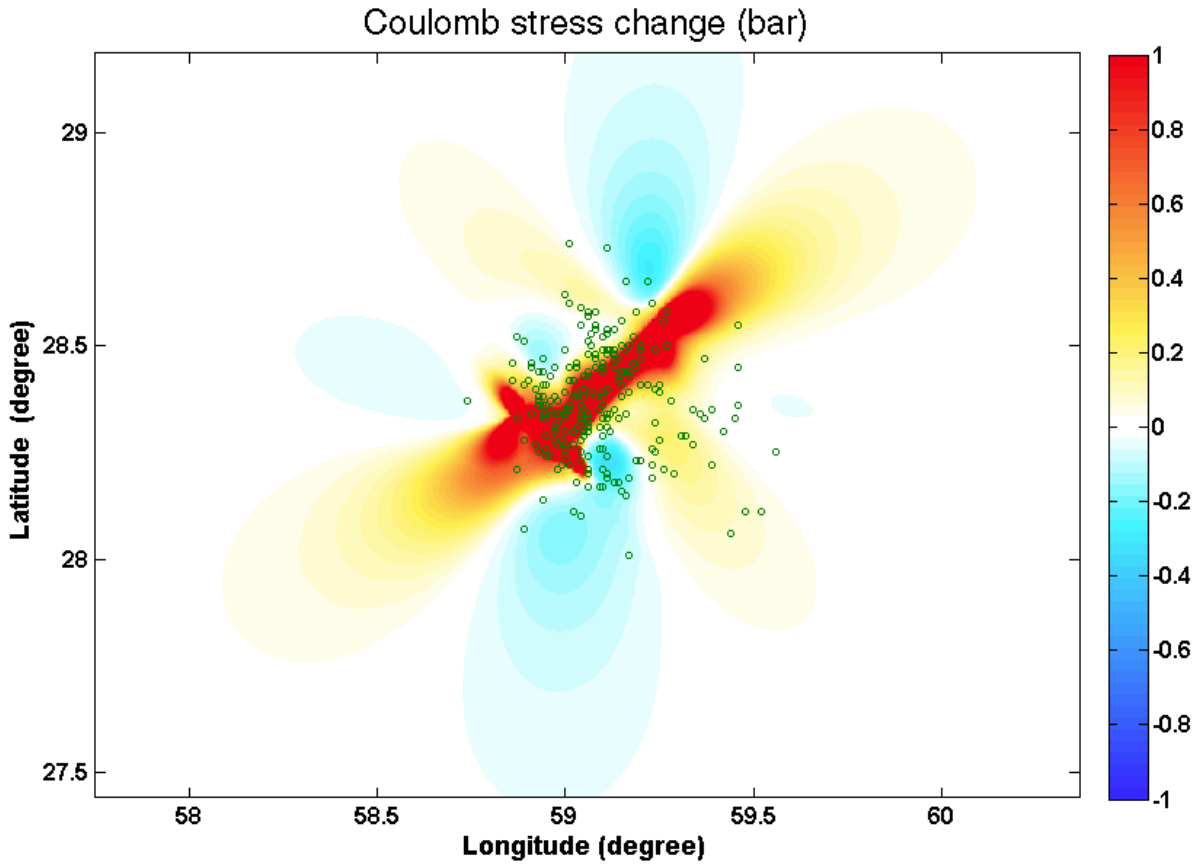

Highlights

1. This study assesses the aftershock activity of two earthquakes that occurred on December 20, 2010 with magnitude of M_N 6.5 (Global CMT M_w 6.5) and January 27, 2011 with magnitude of M_N 6.0 (Global CMT M_w 6.2) in the Rigan region of southeastern Iran.

2. We concentrated on aftershock activity of this sequence with using Statistical properties of aftershocks (b-value of Gutenberg–Richter relation, partitioning of radiated seismic energy, p-value of modified Omori law, and D_C- value of fractal dimension) and I then use the models to calculate the Coulomb stress change

3. The *b*-values of *b*=0.89±0.08 and *b*=0.88±0.08 were calculated for first main shock and second main shock sequence respectively. This suggests that this region is characterized by large differential stress; the genesis of large aftershock activity in a short time interval gives power this.

4. The *p*-values of 1.1±0.12 and 1.1±0.1 were calculated for the main shocks respectively, which imply fast decay rate of aftershocks and high surface heat flux.

5. A value of the spatial fractal dimension (D_c) equal to 2.34 ± 0.03 and 2.54 ± 0.02 for first and second main shocks sequence respectively, which reveals random spatial distribution and source in a two-dimensional plane that is being filled-up by fractures.